# Post-Newtonian Equations for Free-space Laser Communications between Space-based Systems

Jose M. Gambi, Maria L. Garcia del Pino, Jonathan Mosser, and Ewa B. Weinmüller

*Abstract*—The purpose of this paper is to show that the equations for relative motions derived from the two systems of post-Newtonian equations presented here, allow to increase the acquisition, pointing and tracking accuracy when compared to the Newtonian equations aimed to describe free-space laser communications between Low Earth Orbit (LEO) satellites, so as between LEO and Medium Earth Orbit (MEO), and Geostationary Earth Orbit (GEO) satellites. The equations discussed in this work are similar, but not equivalent to those proposed for space debris removal, i. e. in the context of space-based systems to throw middle size LEO debris objects into the atmosphere via laser ablation. In fact, the present equations are computationally much more affordable because the aim is now less demanding, and so they result from subtractions within each post-Newtonian system here provided.

*Keywords*—Free-space communications, laser inter-satellite links, p-N orbital equations.

## I. INTRODUCTION

LASER communications in space are, together with space debris laser ablation, one of the most promising activities in future space missions, which give raise to some subtle issues not solved yet (see e.g. [1], [2]). In particular, accurate space-acquisition, pointing and tracking (APT) laser terminals merit nowadays special attention, since they are to play a prominent role due to the narrow beam widths involved. In fact, these terminals must constitute high precision systems, since it will be essential to keep the sat-to- sat line-of-sight (LOS) and pointing directions as steady as possible, so as to accurately implement the point-ahead angles, especially for long distances [3].

Since the sat-to-sat laser communications, unlike the ground-sat, are free from absorption and other atmospheric phenomena, such as scattering and scintillations, then the main dynamical challenge in establishing reliable sat-to-sat links is to implement these directions and angles after adding the respective post-Newtonian corrections to the standard corrections, such as those due to the oblateness of the Earth, the Lunar-Solar gravities and the solar radiation pressure. In fact, these post-Newtonian corrections provide the accuracy required to yield the best possible actual alinement of transmitters and receivers.

This is the reason why, despite the post-Newtonian framework (of the Earth surrounding space) is more complex than the Newtonian, it has to be used, on this occasion to include these corrections, similarly to the way it is used in space geodesy, navigation, and geolocation (see e.g. [4]−[12]).

Consequently, in order to correctly implement the APT manoeuvres, the relative post-Newtonian orbital equations of the receivers with respect to the emitters have to be derived from the respective post-Newtonian Earth centered inertial (ECI) equations, i.e. from the geodesic equations for the post-Newtonian approximation to the Earth Schwarzschild field. In fact, according to the Riemannian paradigm, these are the only equations which enable to describe the orbital motions for objects in the vicinity of the Earth, independently from the consideration of the standard effects mentioned above [13].

The paper is organized as follows: The post-Newtonian models for the Earth surrounding space considered in this work are introduced in Section II. Moreover, in this section, we derive the two families of ECI equations. The simulations for different satellite configurations can be found in Section III. In these simulations we aim at resembling actual scenarios for laser communication between LEO, MEO, and GEO satellites. The numerical method, differential equations and computational data used in the simulations are also described in this section. We complete the article with Section IV, where concluding remarks are provided.

## II. THE EQUATIONS OF THE RELATIVE MOTIONS

In order to consider simple equations, and yet useful to upper - low bound the post-Newtonian corrections, we initially adopt as geometric model $g_{ab}$ of the Earth surrounding space in ECI coordinates, $x^i$ $(x^\alpha,\ t)$, the first order post-Newtonian expansion of the Earth Schwarzschild field, which is given by

$$
\begin{aligned}
g_{\alpha\beta} &= \delta_{\alpha\beta} + \gamma_{\alpha\beta} + O(\varepsilon^2), \\
g_{\alpha 4} &= O(\varepsilon^{3/2}), \\
g_{44} &= -1 + \gamma_{44} + O(\varepsilon^2),
\end{aligned}
\tag{1}
$$

where

$$
\gamma_{\alpha\beta} = \frac{2m}{r}\frac{x_\alpha x_\beta}{r^2}, \quad \gamma_{44} = \frac{2m}{r}.
\tag{2}
$$

Here, $m$ is the mass of the Earth measured in seconds, $r^2 =$

J. M. Gambi: Gregorio Millan Institute, University Carlos III de Madrid, 28911 Leganes, Madrid, Spain, e-mail: gambi@math.uc3m.es.
M. L. Garcia del Pino: I.E.S. Alpajes, 28300 Aranjuez, Madrid, Spain.
J. Mosser and E. B. Weinm¨uller: Institute for Analysis and Scientific Computing, Vienna University of Technology, A-1040 Wien, Austria.

$x_\alpha x^\alpha$, where $r$ is also measured in seconds ($G = c = 1$), and $\varepsilon \sim O(m/r) \sim O(v^2)$, where $v$ is the characteristic speed of the Earth satellites, and therefore, dimensionless [14]. (Latin indices range from 1 to 4, and Greek, from 1 to 3).

For the reasons discussed in the introduction, the ECI orbital equations for any satellite, say $S$, follow from the geodesic equations,

$$\frac{d^2 x^i}{ds^2} = -\Gamma^i{}_{jk} \frac{dx^j}{ds} \frac{dx^k}{ds}, \tag{3}$$

where $s$ is the proper time of $S$ and $\Gamma^i{}_{jk}$ are the Christoffel symbols of the second kind for the metric (1).

Thus, the space part of this metric, $g_{\alpha\beta}$, is almost Euclidean, $g_{44}$ is almost $-1$, and the Christoffel symbols, $\Gamma^i{}_{jk}$, as for any other metric similar to (1) are

$$\Gamma^i{}_{jk} = \frac{1}{2} \eta^{ia} [\gamma_{ja,k} + \gamma_{ka,j} - \gamma_{jk,a}], \tag{4}$$

where $\gamma_{ja,k} = \partial\gamma_{ja}/\partial x^k$ etc., expanded up to $O(\varepsilon)$ terms.

Then, for the first three equations in (3) we have

$$\frac{d^2 x^\alpha}{ds^2} = \frac{-mx^\alpha}{r^3} \left[ \left( 2\delta_{\beta\gamma} - \frac{3x^\beta x^\gamma}{r^2} \right) \frac{dx^\beta}{ds} \frac{dx^\gamma}{ds} \right.$$
$$\left. + \left( \frac{dx^4}{ds} \right)^2 \right] + O(\varepsilon^2), \tag{5}$$

and for the fourth

$$\frac{d^2 x^4}{ds^2} = \frac{-2m}{r^3} x^\gamma \frac{dx^\gamma}{ds} \frac{dx^4}{ds} + O(\varepsilon^2), \tag{6}$$

so that, by integrating (6) up to $O(\varepsilon)$, we have

$$\left( \frac{dx^4}{ds} \right)^2 = \left( \frac{dt}{ds} \right)^2 = 1 + O(\varepsilon). \tag{7}$$

Then, after inserting (7) into (5), expanding (5), and using (6), the first system of equations (omitting the expression $O(\varepsilon^2)$) reads:

$$\frac{d^2 x}{dt^2} = \frac{-mx}{r^3} \left[ 1 + \left( 2 - \frac{3x^2}{r^2} \right) \left( \frac{dx}{dt} \right)^2 + \left( 2 - \frac{3y^2}{r^2} \right) \left( \frac{dy}{dt} \right)^2 \right.$$
$$\left. + \left( 2 - \frac{3z^2}{r^2} \right) \left( \frac{dz}{dt} \right)^2 - \frac{6xy}{r^2} \frac{dx}{dt} \frac{dy}{dt} - \frac{6xz}{r^2} \frac{dx}{dt} \frac{dz}{dt} - \frac{6yz}{r^2} \frac{dy}{dt} \frac{dz}{dt} \right],$$

$$\frac{d^2 y}{dt^2} = \frac{-my}{r^3} \left[ 1 + \left( 2 - \frac{3x^2}{r^2} \right) \left( \frac{dx}{dt} \right)^2 + \left( 2 - \frac{3y^2}{r^2} \right) \left( \frac{dy}{dt} \right)^2 \right.$$

$$+ \left( 2 - \frac{3z^2}{r^2} \right) \left( \frac{dz}{dt} \right)^2 - \frac{6xy}{r^2} \frac{dx}{dt} \frac{dy}{dt} - \frac{6xz}{r^2} \frac{dx}{dt} \frac{dz}{dt} - \frac{6yz}{r^2} \frac{dy}{dt} \frac{dz}{dt} \right],$$

$$\frac{d^2 z}{dt^2} = \frac{-mz}{r^3} \left[ 1 + \left( 2 - \frac{3x^2}{r^2} \right) \left( \frac{dx}{dt} \right)^2 + \left( 2 - \frac{3y^2}{r^2} \right) \left( \frac{dy}{dt} \right)^2 \right.$$
$$\left. + \left( 2 - \frac{3z^2}{r^2} \right) \left( \frac{dz}{dt} \right)^2 - \frac{6xy}{r^2} \frac{dx}{dt} \frac{dy}{dt} - \frac{6xz}{r^2} \frac{dx}{dt} \frac{dz}{dt} - \frac{6yz}{r^2} \frac{dy}{dt} \frac{dz}{dt} \right], \tag{8}$$

where $x^1 \equiv x$, $x^2 \equiv y$, and $x^3 \equiv z$.

The geometry adopted to derive the second system of ECI equations includes the second order terms that correspond to the rigorous expansion of the Earth Schwarzschild field up to $O(\varepsilon^3)$ terms. The metric deviations, $\gamma_{ab}$, now are

$$\gamma_{\alpha\beta} = \left( \frac{2m}{r} + \frac{4m^2}{r^2} \right) \frac{x_\alpha x_\beta}{r^2}, \quad \gamma_{44} = \frac{2m}{r}, \tag{9}$$

so that we obtain

$$\frac{d^2 x^\alpha}{ds^2} = \frac{-mx^\alpha}{r^3} \left[ \left( 2\delta_{\beta\gamma} - \frac{3x^\beta x^\gamma}{r^2} - \frac{2m}{r} \frac{x^\beta x^\gamma}{r^2} \right) \frac{dx^\beta}{ds} \frac{dx^\gamma}{ds} \right.$$
$$\left. + \left( 1 - \frac{2m}{r} \right) \left( \frac{dx^4}{ds} \right)^2 \right] + O(\varepsilon^3), \tag{10}$$

and

$$\frac{d^2 x^4}{ds^2} = \frac{-2m}{r^3} x^\gamma \left( 1 + \frac{2m}{r} \right) \frac{dx^\gamma}{ds} \frac{dx^4}{ds} + O(\varepsilon^3), \tag{11}$$

from which we have

$$\frac{dt}{ds} = 1 + \frac{m}{r} + \frac{1}{2} v^2 + O(\varepsilon^2). \tag{12}$$

Then, with $O(\varepsilon^3)$ omitted, we finally arrive at the following equations:

$$\frac{d^2 x}{dt^2} = \frac{-mx}{r^3} \left[ 1 - \frac{2m}{r} + \left( 2 - \frac{3x^2}{r^2} - \frac{2m}{r} \frac{x^2}{r^2} \right) \left( \frac{dx}{dt} \right)^2 \right.$$
$$+ \left( 2 - \frac{3y^2}{r^2} - \frac{2m}{r} \frac{y^2}{r^2} \right) \left( \frac{dy}{dt} \right)^2 + \left( 2 - \frac{3z^2}{r^2} - \frac{2m}{r} \frac{z^2}{r^2} \right) \left( \frac{dz}{dt} \right)^2$$
$$\left. + \left( 1 + \frac{2m}{3r} \right) \left( - \frac{6xy}{r^2} \frac{dx}{dt} \frac{dy}{dt} - \frac{6xz}{r^2} \frac{dx}{dt} \frac{dz}{dt} - \frac{6yz}{r^2} \frac{dy}{dt} \frac{dz}{dt} \right) \right]$$
$$+ \frac{2m}{r^3} \left( 1 + \frac{2m}{r} \right) \left( x \frac{dx}{dt} + y \frac{dy}{dt} + z \frac{dz}{dt} \right) \frac{dx}{dt},$$

$$\frac{d^2 y}{dt^2} = \frac{-my}{r^3}\left[1 - \frac{2m}{r} + \left(2 - \frac{3x^2}{r^2} - \frac{2m}{r}\frac{x^2}{r^2}\right)\left(\frac{dx}{dt}\right)^2\right.$$

$$+ \left(2 - \frac{3y^2}{r^2} - \frac{2m}{r}\frac{y^2}{r^2}\right)\left(\frac{dy}{dt}\right)^2 + \left(2 - \frac{3z^2}{r^2} - \frac{2m}{r}\frac{z^2}{r^2}\right)\left(\frac{dz}{dt}\right)^2$$

$$+ \left(1 + \frac{2m}{3r}\right)\left(-\frac{6xy}{r^2}\frac{dx}{dt}\frac{dy}{dt} - \frac{6xz}{r^2}\frac{dx}{dt}\frac{dz}{dt} - \frac{6yz}{r^2}\frac{dy}{dt}\frac{dz}{dt}\right)\right]$$

$$+ \frac{2m}{r^3}\left(1 + \frac{2m}{r}\right)\left(x\frac{dx}{dt} + y\frac{dy}{dt} + z\frac{dz}{dt}\right)\frac{dy}{dt},$$

$$\frac{d^2 z}{dt^2} = \frac{-mz}{r^3}\left[1 - \frac{2m}{r} + \left(2 - \frac{3x^2}{r^2} - \frac{2m}{r}\frac{x^2}{r^2}\right)\left(\frac{dx}{dt}\right)^2\right.$$

$$+ \left(2 - \frac{3y^2}{r^2} - \frac{2m}{r}\frac{y^2}{r^2}\right)\left(\frac{dy}{dt}\right)^2 + \left(2 - \frac{3z^2}{r^2} - \frac{2m}{r}\frac{z^2}{r^2}\right)\left(\frac{dz}{dt}\right)^2$$

$$+ \left(1 + \frac{2m}{3r}\right)\left(-\frac{6xy}{r^2}\frac{dx}{dt}\frac{dy}{dt} - \frac{6xz}{r^2}\frac{dx}{dt}\frac{dz}{dt} - \frac{6yz}{r^2}\frac{dy}{dt}\frac{dz}{dt}\right)\right]$$

$$+ \frac{2m}{r^3}\left(1 + \frac{2m}{r}\right)\left(x\frac{dx}{dt} + y\frac{dy}{dt} + z\frac{dz}{dt}\right)\frac{dz}{dt}.$$

$$(13)$$

### III. NUMERICAL SIMULATIONS

To derive representative corrections, we have taken into account that the LEO zones of 200 km, 400 km, and 800 km are the most frequently used for research, meteorological monitoring and distant probing, respectively [15]. Hence we considered different satellites at these altitudes, *T*1, *T*2, *T*3, aimed to engage with laser beams, and be engaged from, one LEO satellite at high altitude, *S−LEO* (Table I), one MEO satellite, *S − MEO*, with altitude and eccentricity similar to those of the GPS satellites (Table II), and one GEO satellite, *S−GEO* (Table III).

| S-LEO | T1 | T2 | T3 |
|---|---|---|---|
| Alt. at perigee (km) | 200 | 400 | 800 |
| Eccentricity | 0.003 | 0.002 | 0 |
| P-N corr. from (14) (m) | 5.3 | 6.1 | 5.9 |
| P-N corr. from (15) (m) | 4.7 | 4.4 | 3.4 |
| Shuan diameter (m) | 2.7 | 2.4 | 1.8 |
| Phipps diameter (m) | 0.8 | 0.7 | 0.5 |

Table I. Post-Newtonian corrections in one day for *S−LEO*

To facilitate the comparison between the corrections, computed by subtracting the equations for two satellites within each system (equations (8) and (13)) to compare them with the diameters of the beam spots estimated from [16] and [17], all the satellites were assumed to be equatorial. Moreover, the differences between the LOS and pointing directions were neglected. Hence the differential equations used to estimate the post-Newtonian corrections for the relative motions of the *T−Satellites* with respect to each *S* were

$$\frac{d^2 X}{dt^2} = \frac{-mx_T}{r_T^3}\left[1 + \left(2 - \frac{3x_T^2}{r_T^2}\right)\left(\frac{dx_T}{dt}\right)^2 + \left(2 - \frac{3y_T^2}{r_T^2}\right)\left(\frac{dy_T}{dt}\right)^2\right.$$

$$\left. - \frac{6x_T y_T}{r_T^2}\frac{dx_T}{dt}\frac{dy_T}{dt}\right] + \frac{mx_S}{r_S^3}\left[1 + \left(2 - \frac{3x_S^2}{r_S^2}\right)\left(\frac{dx_S}{dt}\right)^2\right.$$

$$\left. + \left(2 - \frac{3y_S^2}{r_S^2}\right)\left(\frac{dy_S}{dt}\right)^2 - \frac{6x_S y_S}{r_S^2}\frac{dx_S}{dt}\frac{dy_S}{dt}\right],$$

$$\frac{d^2 Y}{dt^2} = \frac{-my_T}{r_T^3}\left[1 + \left(2 - \frac{3x_T^2}{r_T^2}\right)\left(\frac{dx_T}{dt}\right)^2 + \left(2 - \frac{3y_T^2}{r_T^2}\right)\left(\frac{dy_T}{dt}\right)^2\right.$$

$$\left. - \frac{6x_T y_T}{r_T^2}\frac{dx_T}{dt}\frac{dy_T}{dt}\right] + \frac{my_S}{r_S^3}\left[1 + \left(2 - \frac{3x_S^2}{r_S^2}\right)\left(\frac{dx_S}{dt}\right)^2\right.$$

$$\left. + \left(2 - \frac{3y_S^2}{r_S^2}\right)\left(\frac{dy_S}{dt}\right)^2 - \frac{6x_S y_S}{r_S^2}\frac{dx_S}{dt}\frac{dy_S}{dt}\right],$$

$$(14)$$

and

$$\frac{d^2 X}{dt^2} = \frac{-mx_T}{r_T^3}\left[1 - \frac{2m}{r_T} + \left(2 - \frac{3x_T^2}{r_T^2} - \frac{2m}{r_T}\frac{x_T^2}{r_T^2}\right)\left(\frac{dx_T}{dt}\right)^2\right.$$

$$+ \left(2 - \frac{3y_T^2}{r_T^2} - \frac{2m}{r_T}\frac{y_T^2}{r_T^2}\right)\left(\frac{dy_T}{dt}\right)^2 - \left(1 + \frac{2m}{3r_T}\right)\left(\frac{6x_T y_T}{r_T^2}\frac{dx_T}{dt}\frac{dy_T}{dt}\right)\right]$$

$$+ \frac{2m}{r_T^3}\left(1 + \frac{2m}{r_T}\right)\left(x_T\frac{dx_T}{dt} + y_T\frac{dy_T}{dt}\right)\frac{dx_T}{dt}$$

$$+ \frac{mx_S}{r_S^3}\left[1 - \frac{2m}{r_S} + \left(2 - \frac{3x_S^2}{r_S^2} - \frac{2m}{r_S}\frac{x_S^2}{r_S^2}\right)\left(\frac{dx_S}{dt}\right)^2\right.$$

$$+ \left(2 - \frac{3y_S^2}{r_S^2} - \frac{2m}{r_S}\frac{y_S^2}{r_S^2}\right)\left(\frac{dy_S}{dt}\right)^2 - \left(1 + \frac{2m}{3r_S}\right)\left(\frac{6x_S y_S}{r_S^2}\frac{dx_S}{dt}\frac{dy_S}{dt}\right)\right]$$

$$- \frac{2m}{r_S^3}\left(1 + \frac{2m}{r_S}\right)\left(x_S\frac{dx_S}{dt} + y_S\frac{dy_S}{dt}\right)\frac{dx_S}{dt},$$

$$\frac{d^2 Y}{dt^2} = \frac{-my_T}{r_T^3}\left[1 - \frac{2m}{r_T} + \left(2 - \frac{3x_T^2}{r_T^2} - \frac{2m}{r_T}\frac{x_T^2}{r_T^2}\right)\left(\frac{dx_T}{dt}\right)^2\right.$$

$$+ \left(2 - \frac{3y_T^2}{r_T^2} - \frac{2m}{r_T}\frac{y_T^2}{r_T^2}\right)\left(\frac{dy_T}{dt}\right)^2 - \left(1 + \frac{2m}{3r_T}\right)\left(\frac{6x_T y_T}{r_T^2}\frac{dx_T}{dt}\frac{dy_T}{dt}\right)\right]$$

$$+ \frac{2m}{r_T^3}\left(1 + \frac{2m}{r_T}\right)\left(x_T\frac{dx_T}{dt} + y_T\frac{dy_T}{dt}\right)\frac{dy_T}{dt}$$

$$+ \frac{my_S}{r_S^3}\left[1 - \frac{2m}{r_S} + \left(2 - \frac{3x_S^2}{r_S^2} - \frac{2m}{r_S}\frac{x_S^2}{r_S^2}\right)\left(\frac{dx_S}{dt}\right)^2\right.$$

$$+ \left(2 - \frac{3y_S^2}{r_S^2} - \frac{2m}{r_S}\frac{y_S^2}{r_S^2}\right)\left(\frac{dy_S}{dt}\right)^2 - \left(1 + \frac{2m}{3r_S}\right)\left(\frac{6x_S y_S}{r_S^2}\frac{dx_S}{dt}\frac{dy_S}{dt}\right)\right]$$

$$- \frac{2m}{r_S^3}\left(1 + \frac{2m}{r_S}\right)\left(x_S\frac{dx_S}{dt} + y_S\frac{dy_S}{dt}\right)\frac{dy_S}{dt},$$

$$(15)$$

respectively, where $(x_T, y_T)$, $(x_S, y_S)$ are the ECI coordinates of

the $T-Satellites$ and of each $S$, respectively, $r_T^2 = x_T^2 + y_T^2$, $r_S^2 = x_S^2 + y_S^2$, and $(X,Y)$ are the coordinates of the $T-Satellites$ with respect to the $S$'s considered.

The eccentricities and altitudes at perigee of the $S-LEO$ and $S-MEO$ considered in Tables I and II were 0:001, 2000 km, and 0:003, 20189:16 km respectively. Table III collects the information for $S-GEO$. The data of $T1$, $T2$ and $T3$ are specified in the respective tables. The diameters of the beam spots correspond to the distances between perigees and are also specified in the tables. Finally, to allow for estimations at the different time intervals usually considered to update the ephemeris, the post-Newtonian corrections derived from (14) and (15) are listed in meters for a simulation time of one day.

| S-MEO | T1 | T2 | T3 |
|---|---|---|---|
| Alt. at perigee (km) | 200 | 400 | 800 |
| Eccentricity | 0.002 | 0.001 | 0 |
| P-N corr. from (14) (m) | 7.1 | 6.9 | 5.7 |
| P-N corr. from (15) (m) | 5.5 | 4.9 | 4.2 |
| Shuan diameter (m) | 30 | 29.7 | 29.1 |
| Phipps diameter (m) | 8.8 | 8.7 | 8.5 |

Table II. Post-Newtonian corrections in one day for $S-MEO$

| S-GEO | T1 | T2 | T3 |
|---|---|---|---|
| Alt. at perigee (km) | 200 | 400 | 800 |
| Eccentricity | 0.002 | 0.001 | 0 |
| P-N corr. from (14) (m) | 7.1 | 6.8 | 5.8 |
| P-N corr. from (15) (m) | 5.4 | 4.9 | 4.2 |
| Shuan diameter (m) | 52.8 | 52.5 | 51.9 |
| Phipps diameter (m) | 15.5 | 15.4 | 15.2 |

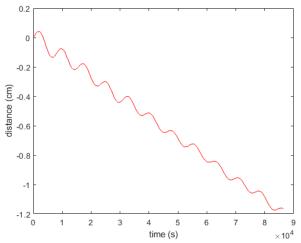Table III. Post-Newtonian corrections in one day for $S-GEO$



Fig. 1 radial distance from ECI Newtonian to post-Newtonian positions of $S-LEO$ from (15)

Figs. 1 to 8 present results of the simulations involving $S-LEO$, and Figs 9 to 16 some others corresponding to $S-GEO$.

Fig. 1 shows the radial distance from the ECI center between the ECI Newtonian and post-Newtonian positions of

$S-LEO$, computed using (15).

Analogously, Fig. 2 shows the radial distance between the ECI Newtonian and post-Newtonian positions of $T2$, cf. Table I, computed from (15). In Fig. 3, the Newtonian and the two post-Newtonian orbits of $T2$ (see Table I) with respect to $S-LEO$ are shown, calculated from (14) and (15). Here, the reference equations were the Newtonian equations for a spherical Earth. Fig. 4 shows the zoomed in end portion of these orbits.
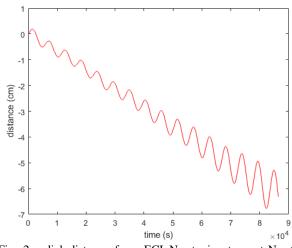


Fig. 2 radial distance from ECI Newtonian to post-Newtonian positions of $T2$, Table I (from (15)
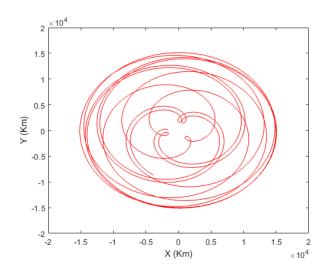


Fig. 3 Newtonian and post-Newtonian orbits of $T2$, Table I, w.r.t. $S-LEO$ (from Newtonian equations and (14), (15))

In Fig. 5 the post-Newtonian corrections to the Newtonian position of $T2$, again cf. Table I, with respect to $S-LEO$ versus time are depicted. They were computed from (14). In Fig. 6, we can see the post-Newtonian corrections, also for one day of simulation, to the Newtonian position of $T2$, see Table I, with respect to $S-LEO$ versus time, computed from (15).
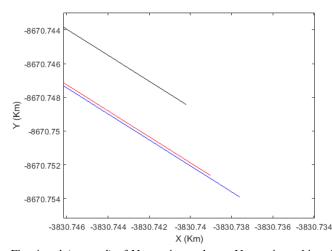
Fig. 4 end (zoomed) of Newtonian and post-Newtonian orbits of *T2*, Table I, w.r.t. *S−LEO* (from Newtonian equations and (14), (15))
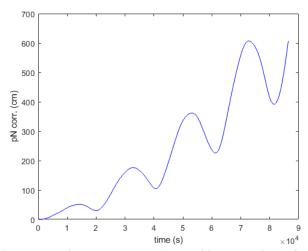


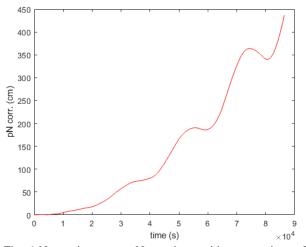Fig. 5 Newtonian to post-Newtonian position corrections of *T2*, Table I, w.r.t. *S−LEO* vs. time (from (14))



Fig. 6 Newtonian to post-Newtonian position corrections of *T2*, Table I, w.r.t. *S−LEO* vs. time (from (15))

Fig. 7 shows the post-Newtonian corrections to the

Newtonian position of *T2* (Table I) with respect to *S−LEO* versus the distance, *d*, between *S−LEO* and *T2*. The data were computed using (14). Fig. 8 shows the post-Newtonian corrections to the Newtonian position of *T2* (Table I) with respect to *S−LEO* versus distance between *S−LEO* and *T2*, computed from (15).
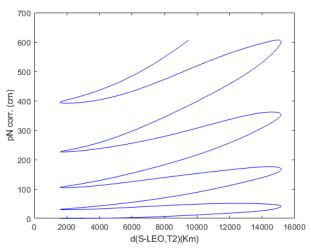


Fig. 7 Newtonian to post-Newtonian position corrections of *T2*, Table I, w.r.t. *S−LEO* vs. distance(*S−LEO,T2*) (from (14))
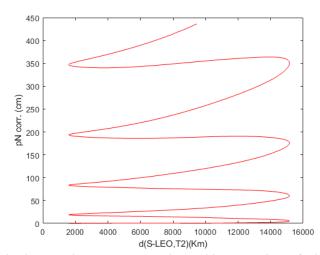


Fig. 8 Newtonian to post-Newtonian position corrections of *T2*, Table I, w.r.t. *S−LEO* vs. distance(*S−LEO,T2*) (from (15))

Fig. 9 shows the radial distances from the ECI center between the ECI Newtonian and post-Newtonian positions of *S− GEO*, computed from (14) (blue) and (15) (red). Analogously to Fig. 3, Fig. 10 shows the Newtonian and the two post-Newtonian orbits of *T2* (see Table III) with respect to *S−GEO*, calculated from (14) and (15). Here, as in Fig. 3, the reference equations were the Newtonian equations for a spherical Earth. Fig. 11 shows the post-Newtonian relative velocity of *T2* (Table III) with respect to *S−GEO*, derived from (14). Fig 12 shows the post-Newtonian corrections to the Newtonian position of *T2* (Table III) with respect to *S−GEO* versus the distance, *d*, between *S−GEO* and *T2*. The results were computed from (14) (blue) and (15) (red).

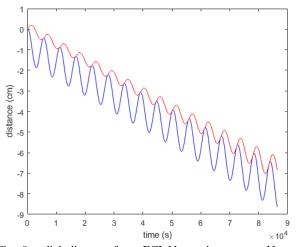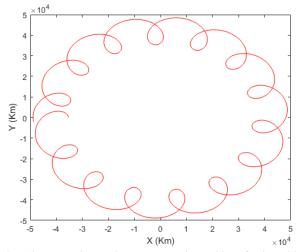Fig. 9 radial distance from ECI Newtonian to post-Newtonian positions of *S−GEO* from (14) and (15)



Fig. 12 Newtonian to post-Newtonian position corrections of *T2*, Table III, w.r.t. *S−GEO* vs. distance(*S−GEO*,*T2*) (from (14),(15))



Fig. 10 Newtonian and post-Newtonian orbits of *T2*, Table III, w.r.t. *S−GEO* (from Newtonian equations and (14), (15))
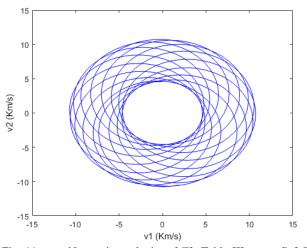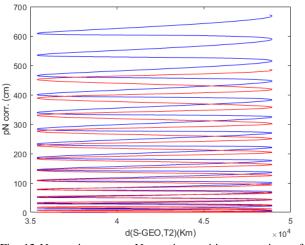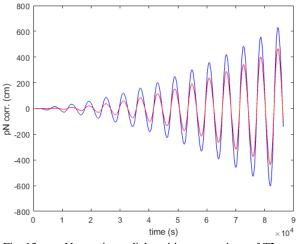


Fig. 13 post-Newtonian radial position corrections of *T2*, Table III, w.r.t. *S−GEO* vs. time (from (14),(15))



Fig. 11. post-Newtonian velocity of *T2*, Table III, w.r.t. *S−LGEO* (from (14))



Fig. 14 post-Newtonian radial position corrections of *T2* w.r.t. *S−GEO* vs. *d*(*S−GEO*,*T2*) (from (14),(15))

Figs. 13 and 14 show the radial post-Newtonian corrections

to the Newtonian position of *T2* (Table III) with respect to

*S− GEO* versus time and distance, *d*, from *S− GEO* to *T2,* respectively, computed from (14) (blue) and (15) (red). Finally, Figs. 15 and 16 show the transverse post-Newtonian corrections to the Newtonian position of *T2* (Table III) with respect to *S−GEO* versus time and distance, *d*, from *S−GEO* to *T2,* respectively, computed from (14) (blue) and (15) (red).
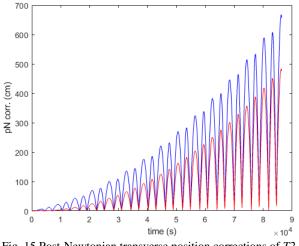


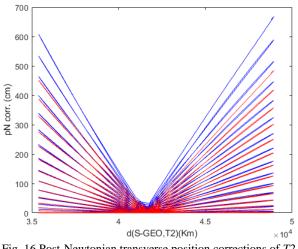Fig. 15 Post-Newtonian transverse position corrections of *T2*, Table III, w.r.t. *S−GEO* vs. time (from (14),(15))



Fig. 16 Post-Newtonian transverse position corrections of *T2*, Table III, w.r.t. *S−GEO* vs. *d*(*S−GEO*,*T2*) (from (14),(15))

Both the ECI and relative orbits corresponding to (8), (13) and (14), (15) were computed using the MATLAB standard routine ode45 for the approximation of initial value problems (IVPs) in first order ordinary differential equations. Since the systems in (8), (13) and (14), (15) are of the second order, they were first transformed to related systems of the first order. The latter were then completed by a proper set of initial conditions. The ode45 solver is based on the Dormand-Prince method [18] including two explicit RungeKutta methods of order four and five and requiring six function evaluations per step. After each step, the difference between these solutions is taken to estimate the local error of the fourth order solution. This error estimate

is then used to adapt the length of the step-size in such a way that the tolerance requirements provided by the user are satisfied. The Dormand-Prince method has seven stages, but it uses only six function evaluations per step because it has the First Same As Last property: the last stage is evaluated at the same point as the first stage of the next step. The coefficients of the method are chosen to minimize the error of the fifth order solution. All calculation presented in the paper were carried out using the absolute and relative error control with the tolerance requirements set to $TOLa = TOLr = 10^{-11}$.

In a typical run, the whole interval of integration was split into 3000 equidistant subintervals. Starting from the first subinterval, an IVP was solved on an adapted grid until the end of the first subinterval was reached, and the code delivered an approximation of the prescribed accuracy. This procedure was repeated in the following subintervals, always starting with final solution values of the proceeding subinterval.

Finally, we stress that the experiments carried out here were not optimized for the *practical* production runs; our aim was merely to illustrate the importance of the post-Newtonian corrections.

## IV. CONCLUSION

Aside from the expected result that, as can be observed in Tables I to III, the relative corrections for the LOS and pointing directions between LEO satellites are the largest, the most relevant conclusion that can be derived from this work follows from the hypothesis made to derive (14) and (15). In fact, from this analysis it can be positively concluded that the differences between the post-Newtonian corrections for the LOS and pointing directions shown in the tables, and in Figs. 5 to 8, are mainly due to the hypothesis in (7) and (12). In other words, they are due to the basic assumption that, according to (7), the ECI time coordinate is almost absolute and, according to. (12), it is not. Clearly, both hypothesis are truly post-Newtonian, since they are consistent with the order of the expansions considered in each case, although obviously, the second is closer to the principles of general relativity. Consequently, from the point of view of this theory, the corrections predicted from (14) can only be considered as upper-bounds for the corrections deduced using (15), cf. the beginning of Section III. Therefore, we conclude that to obtain corrections similar to those derived here from (15), only those satellites with atomic clocks on board can be used.

REFERENCES

[1] J. M. Gambi, M. L. Garcia del Pino, J. Gschwindl, and E. B. Weinmüller, "Post-Newtonian equations of motion for LEO debris objects and space-based acquisition, pointing and tracking laser systems", *Acta Astronautica*, vol. 141, pp 132-142, Dic 2017.

[2] R. Amofa, B. Declercq, and J. Engelen, "Optical Communication in Space.doc", *Studieopdracht voor het vak Optische Communicatie. Prof. J. Engelen. Academiejaar*", 2004-2005, hannah.be.

[3] Q. L. Hu, Z. H. Li, K. Qiao, and X. J. Zhang, "Overview of research on space laser communications tracking and pointing technology", *Chemical Engineering Transactions*, vol. 46, pp. 1015-1020, 2015.

[4] H. Moritz and B. Hofmann-Wellenhof, *Geometry, Relativity, Geodesy*. H. Wichmann Verlag GmbH, 1993), Ch. 5.

[5]   T. B. Bahder,"Navigation in Curved Space-time", *Am. J. Phys.*, vol. 69, pp. 315-321, 2001.

[6]   N. Ashby, *Relativity in the Global Positioning System*, Living Rev. Relativity,  vol. 6 pp. 1, 2003.

[7]   N. Ashby and P. L. Bender, "Measurement of the Shapiro Time Delay between Drag-Free Spacecraft" in *Laser, clocks and drag-free control: exploration of relativistic gravity space*, H. Dittus, C. L¨ammerzahl, and S. G. Turyshev Eds.: Springer, 2007.

[8]   T. B. Bahder, "Clock Synchronization and Navigation in the Vicinity of the Earh", *Nova Science Pub. Inc*., 2009.

[9]   J. M. Gambi, M. C. Rodriguez-Teijeiro, M. L. Garcia del Pino, and M. Salas, "Shapiro time-delay within the Geolocation Problem by TDOA", *IEEE Trans. Aerospace and Electronic Systems*, vol. 47, n. 3, pp. 1948-1962, 2011.

[10]   J. M. Gambi, J. Clares, and M. L. Garcia del Pino, "FDOA post-Newtonian Equations for the Location of Passive Emitters Placed in the Vicinity of the Earth", *Aerospace Science and Technology*, vol. 46, pp. 137-145, 2015.

[11]   J. M. Gambi, J. Clares, and M. C. Rodriguez-Teijeiro, "Post-Newtonian Geolocation of Passive Radio transmitters by TDOA and FDOA", in *Progress in Industrial Mathematics at ECMI 2014. Mathematics in Industry 21*. Springer, Heidelberg, Dordrecht, London, New York, 2016.

[12]   J. M. Gambi, M. C. Rodriguez-Teijeiro, and M. L. Garcia del Pino, "Newtonian and post-Newtonian Passive Geolocation by TDOA, *Aerospace Science and Technology*, vol. 51, pp 18-25, 2016.

[13]   M. H. Soffel, *Relativity in Astrometry, Celestial Mechanics and Geodesy*, Astronomy and Astrophysics Library, Springer- Verlag, 1989.

[14]   J. L. Synge, *Relativity: The General Theory*, North-Holland, 1960, Ch. 7, pp. 266.

[15]   M. Shmitz, S. Fasoulas and J. Utzmann, "Performance model for spacebased laser debris sweepers"*, Acta Astronaut.*, vol. 115, pp. 376-383, 2015.

[16]   S. Shuangyan, J. Xing and C. Hao,"Cleaning Space Debris with a Spacebased Laser System", *Chinese Journal of Aeronautics*, vol. 24,n. 4, pp. 805- 811, 2014.

[17]   C. R. Phipps, *L'ADROIT-"*A Spaceborne utraviolet laser system for space debris clearing", *Acta Astronautica*, vol.104, pp. 243-255, 2014.

[18]    J. R. Dormand and P. J. Prince, "A family of embedded Runge-Kutta formulae", *J. Comput. Appl. Math*., vol. 6, n. 1, pp. 19-26, 1980.